Nucleation and dissociation of methane clathrate embryo at the gas–water interface

Rongda Liang[a,1], Huijie Xu[a,1], Yuneng Shen[a], Shumei Sun[a], Jiyu Xu[b], Sheng Meng[b], Y. Ron Shen[a,c,2], and Chuanshan Tian (田传山)[a,d,2]

[a]Department of Physics, State Key Laboratory of Surface Physics and Key Laboratory of Micro- and Nano-Photonic Structure, Fudan University, 200433 Shanghai, China; [b]Beijing National Laboratory for Condensed Matter Physics and Institute of Physics, Chinese Academy of Sciences, 100190 Beijing, China; [c]Department of Physics, University of California, Berkeley, CA 94720; and [d]Collaborative Innovation Center of Advanced Microstructures, 210093 Nanjing, China

Contributed by Y. Ron Shen, September 18, 2019 (sent for review July 22, 2019; reviewed by Eric Borguet and Feng Wang)

Among natural energy resources, methane clathrate has attracted tremendous attention because of its strong relevance to current energy and environment issues. Yet little is known about how the clathrate starts to nucleate and disintegrate at the molecular level, because such microscopic processes are difficult to probe experimentally. Using surface-specific sum-frequency vibrational spectroscopy, we have studied in situ the nucleation and disintegration of methane clathrate embryos at the methane-gas–water interface under high pressure and different temperatures. Before appearance of macroscopic methane clathrate, the interfacial structure undergoes 3 stages as temperature varies, namely, dissolution of methane molecules into water interface, formation of cage-like methane–water complexes, and appearance of microscopic methane clathrate, while the bulk water structure remains unchanged. We find spectral features associated with methane–water complexes emerging in the induction time. The complexes are present over a wide temperature window and act as nuclei for clathrate growth. Their existence in the melt of clathrates explains why melted clathrates can be more readily recrystallized at higher temperature, the so-called "memory effect." Our findings here on the nucleation mechanism of clathrates could provide guidance for rational control of formation and disintegration of clathrates.

methane clathrate | gas–water interface | nucleation | sum-frequency vibrational spectroscopy

Clathrate hydrates are compound crystals composed of hydrogen-bonding cages of water molecules entrapping guest molecules, such as methane. They have many important applications related to energy and environment (1–10). For example, formation of clathrate hydrates could be a viable means for sequestration of CO_2 (5, 11) and storage and transportation of natural gas (4, 7). It can also cause serious safety problems for flow assurance in oil and gas pipelines (4). More importantly, the vast amount of methane clathrate naturally deposited on the ocean floor is among the most readily accessible, nearly inexhaustible, new energy resources on earth (12).

Formation of clathrate hydrates undergoes a microscopic nucleation stage (9, 13) followed by a macroscopic growth process. While the latter has been well studied by various means (14), the molecular-level understanding of their nucleation kinetics, essential for promotion and inhibition of the solid form in the aforementioned issues (9, 15), still remains elusive. Most microscopic studies of nucleation of such hydrates in the past decades have been carried out by molecular-dynamic simulations (1–3, 6, 16–18) of supersaturated solution of guest molecules in water with unrealistically high driving force (19), and their predictions are difficult to be experimentally verified (8, 14). Note that most of the guest molecules for the clathrate hydrates are hardly soluble in water. Their nucleation and growth with water encompassing gas molecules from dilute gas–water mixture is obviously difficult. Macroscopic observations indicated that clathrate hydrates tend to initially form at the gas–water interface where the guest molecules are more abundant (20, 21). Unfortunately, experimental investigation of interfacial nucleation has been very challenging (9, 22), providing little microscopic information about the evolving growth process before and during nucleation (8).

Among known clathrates, methane clathrate as fuel has received particular attention because of current rush in searching for new energy resources (4, 6). Most of the naturally formed methane clathrates have the so-called s-I structure, the unit cell of which consists of 46 H-bonded water molecules in the form of 2 small cages and 6 large ones, with a methane molecule trapped in each of them (4). According to molecular-dynamics (MD) simulations (9, 23–25), methane with a mole fraction of ∼0.15 in water, which is more than 100× higher than that of methane concentration in water under 5 to 8 MPa of methane gas, would form methane–water clusters with cage-like structure. After reaching a critical size, the clusters can transform first into amorphous and then into crystalline clathrate. However, these simulations were conducted under unrealistic temperature and pressure, with which the nucleation kinetics could be very different from that in real experiment. On the other hand, although the methane concentration in bulk water is highly dilute even under high methane vapor pressure, it was believed that at a high-pressure gas–water interface, the methane solubility can increase to the extent that methane

Significance

Clathrate hydrates are of great current interest because of their relevance to energy and environment. Methane clathrate has attracted particular attention for being the world's largest natural gas resources beneath permafrost and ocean sediments. Yet nucleation of clathrate is still a poorly understood process although its knowledge is crucial for control of clathrate formation and dissociation in many applications. In this work, we used sum-frequency vibrational spectroscopy to probe water under high-pressure methane vapor, and found that nucleation and growth of methane clathrates start at methane–water interface. The spectral change with lowering temperature showed evidence that similar to usual crystal growth, clathrates begin to form when nuclei of cage-like methane–water complex structure at the water interface reach critical size.

Author contributions: C.T. designed research; R.L., H.X., Y.S., S.S., J.X., S.M., and C.T. performed research; R.L., H.X., S.M., Y.R.S., and C.T. analyzed data; and R.L., H.X., Y.R.S., and C.T. wrote the paper.

Reviewers: E.B., Temple University; and F.W., University of Arkansas.

The authors declare no competing interest.

[1]R.L. and H.X. contributed equally to this work.

[2]To whom correspondence may be addressed. Email: yrshen@berkeley.edu or cstian@fudan.edu.cn.

This article contains supporting information online at www.pnas.org/lookup/suppl/doi:10.1073/pnas.1912592116/-/DCSupplemental.

First published November 5, 2019.

clathrate would grow at sufficiently low temperature first at the interface (Fig. 1*A*) and then continuously into the bulk (4). This could be the scenario for the formation of naturally deposited methane clathrate at the bottom of oceans originating from methane gas released from the ocean floor in the form of gas bubbles in water. Indeed, clathrate growth initiated from the gas–water interface could be observed visually (21) and by laser (26), X-ray (27), and neutron scattering (26, 28–30). Unfortunately, very limited microscopic information about the nucleation process could be extracted from these experiments as well as other experiments using Raman scattering (31, 32) and NMR (33, 34). Difficulty lies in the lack of surface specificity of such techniques. In recent years, surface-specific sum-frequency vibrational spectroscopy (SFVS) has been developed into a unique analytical tool for probing gas/liquid interfaces (35), and should be ideal for in situ monitoring of evolution of methane clathrate embryos at the methane–water interface under high pressure during the induction time.

We report here a study using SFVS to probe in situ nucleation and dissociation kinetics of methane clathrate embryos at the methane–water interface under high methane vapor pressure and with different temperatures. Observed spectral changes from the interface allowed us to identify 3 stages of nucleation and dissociation of methane clathrate at the gas–water interface without the presence of bulk clathrate: oversaturated dissolution of methane molecules in the interfacial water layer, appearance of methane–water complex, and presence of microscopic methane clathrate. The characteristic vibrational feature of cage-like structure showed up with the emergence of methane–water complex. As the intermediate species first appearing during the induction time, it was quite robust upon heating once formed. Such species, when present, seemed to facilitate growth of methane clathrate, and could explain the puzzling "memory effect" (22), that is, recrystallization of methane clathrate from the melt can happen at significantly higher temperature because methane clathrate melt contains residual methane–water complexes that have not been dissociated in the melting process. More generally, our investigation provides a detailed microscopic picture of the nucleation and dissociation process of clathrates that will be helpful as guidance for rational control of their formation and disintegration in many applications.

Results and Discussion

Interfacial and Bulk Spectra of Polycrystalline Methane Clathrate. To learn about the interfacial structure of methane–water, we measured the SF spectrum of OD (oxygen-deuterium) stretching vibrations at the methane–D_2O interface; the choice of D_2O instead of H_2O was to avoid strong absorption of the IR input by methane on its way to access the interface. For comparison, we recorded simultaneously the Raman spectrum of the bulk. Fig. 1*A* gives a sketch of the experimental geometry. We first carried out measurement on a polycrystalline methane–D_2O clathrate film grown on a fused silica window as a reference. The observed SF intensity spectrum, $\left|\chi_S^{(2)}(\omega_{IR})\right|^2$, with $\chi_S^{(2)}(\omega_{IR})$ being the surface nonlinear susceptibility, and Raman spectrum are presented in Fig. 1 *B* and *C*, respectively. The latter is essentially the same as those of the s-I structure reported in the literature (36), and the former shows close resemblance to the latter. In the H-bonded OD stretching region, 2 overlapping broad bands centered at ~2,350 cm^{-1} (low-frequency band, LFB) and ~2,520 cm^{-1} (high-frequency band, HFB) are seen. They originate from OD stretches of water molecules more

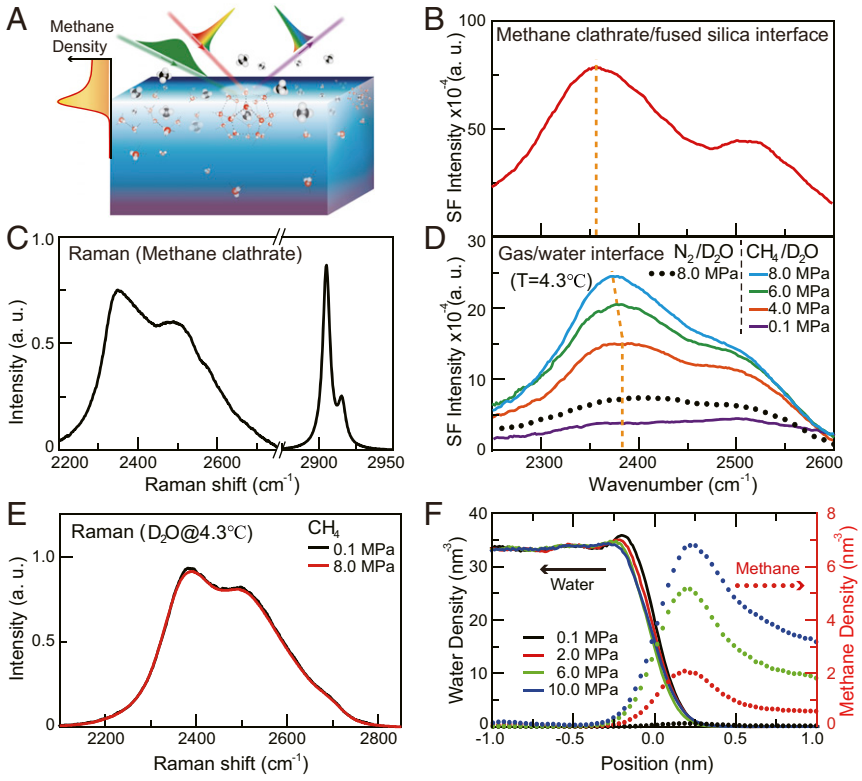

Fig. 1. Spectral characterization of solid methane clathrate and the high-pressure methane–water interface. (*A*) Schematic of SFVS arrangement for probing the methane–water interface. (*Inset, Left*) Density profile of methane in the interfacial region. (*B*) SF spectrum of polycrystalline methane–D_2O clathrate grown on fused silica. (*C*) Raman spectrum of the same sample as in *B*, showing characteristic feature of the s-I crystalline clathrate. (*D*) SF spectra of methane–water (D_2O) interface at 4.3 °C with different methane pressures from 0.1 to 8.0 MPa. SF spectrum of 8.0 MPa nitrogen–D_2O interface (dotted curve) is also presented for comparison. (*E*) Raman spectra of bulk water (D_2O) at 4.3 °C under methane pressures of 0.1 and 8.0 MPa. (*F*) Calculated molecular density profiles of water and methane in the interfacial region versus pressure by MD simulations described in *SI Appendix*.

and less-strongly H-bonded to neighbors, respectively. Note that the LFB in the SF spectrum is redshifted by ~25 cm^{-1} from the corresponding LFB of the vapor–liquid water interface (37, 38). This redshift of the LFB, and the higher intensity of the LFB compared to the HFB, are also seen when liquid water turns into ice (39), indicating a better long-range order of the H-bonding network in the crystalline clathrate. In the clathrate case, these features arise from ordered structure of water forming clathrate cages.

Nucleation of Methane Clathrate at the Gas–Water Interface. We can use the SF spectrum of polycrystalline methane clathrate as a reference in our research for an understanding of the SF spectra of the methane–water interface. Fig. 1*D* presents a set of SF intensity spectra, taken at 4.3 °C under methane vapor pressures of 0.1 (the ambient pressure), 4.0, 6.0, and 8.0 MPa. The spectral intensity is higher at higher pressure; with the LFB grown more than the HFB. At 6.0 and 8.0 MPa, the LFB appears redshifted and becomes more like that of polycrystalline methane clathrate in Fig. 1*B*. In contrast, the Raman spectrum, which characterizes the bulk, shows little change when the pressure increases from 0.1 to 8.0 MPa, as depicted in Fig. 1*E*. The formation of methane clathrate with significant density of dissolved molecules only appears at the water interface, but not in the bulk water, agrees well with the calculated density profiles of methane at the water interface under different gas pressures shown in Fig. 1*F*; details of the calculation are given in *SI Appendix*. We also show in Fig. 1*D* the spectrum of the N_2–water interface under 8.0 MPa of N_2 (dotted curve) for comparison. As expected, because nitrogen clathrate formation requires much higher pressure than methane (40), the spectrum under 8.0 MPa N_2 exhibits only a relatively weak increase in intensity.

In order to see more clearly how methane clathrate evolves at the interface, we measured the SF spectrum of the methane–water interface under fixed methane gas pressure at 8.0 MPa but with temperature varied from 20.6 °C down to −0.5 °C (41). The observed spectra at different times after the temperature started to lower are displayed in Fig. 2*A*. As temperature decreases below ~10 °C, the LFB continuously grows and the spectrum becomes more like that of the crystalline clathrate (Fig. 1*B*), suggesting onset of nucleation of microscopic methane clathrate at ~10 °C. For quantitative analysis, the spectra can generally be fit by a composition of 3 Lorentzian-shaped modes with fixed center frequency and linewidth but adjustable amplitude. (See *SI Appendix* for details.) Two of them at 2,535 and 2,370 cm^{-1} are taken to be the same as those in the spectrum of the gas–water interface at room temperature under 8.0 MPa methane (the 20.6 °C trace in Fig. 2*A*), and in fact, they are the only modes needed to fit the observed spectra above ~10 °C. The third mode, taken to be at the same frequency of 2,350 cm^{-1} as that of the low-frequency mode of polycrystalline methane clathrate shown in Fig. 1*B*, is needed to fit the spectra below ~10 °C, suggesting appearance of microscopic clathrate-like structure at the interface. We emphasize that this 2,350 cm^{-1} mode in the SF spectra came from the methane–water interface, as it was absent in our Raman spectra for the bulk.

The amplitudes of the different modes obtained from fitting the spectra at different temperatures are listed in *SI Appendix*, Table S1 and plotted in Fig. 2*B*. We notice that their variation with temperature can be divided into 3 regions, which are also perceptible from the spectral variation in Fig. 2*A*: Above 14.7 ± 0.5 °C, the strengths of both 2,535 cm^{-1} and 2,370 cm^{-1} modes increase with decrease of temperature, and show little change between ~10 and 14.7 °C. (Note that the amplitude of the 2,535 cm^{-1} mode is negative in sign.) The strengths of the 2,370 cm^{-1} and 2,535 cm^{-1} modes then decrease as temperature decreases below ~10 °C, but the 2,350 cm^{-1} mode emerges and grows. These 3 regions can be identified with 3 structural stages of methane–water mixture in the nucleation process of methane clathrate

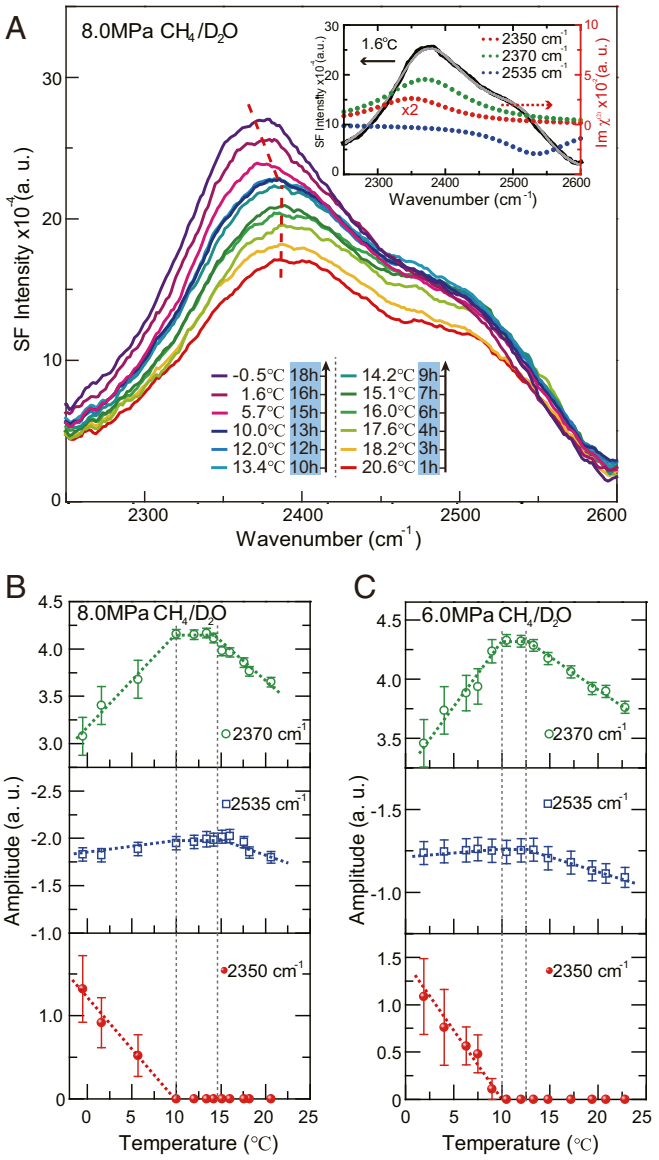

Fig. 2. Temperature dependence of SF spectra at the methane–D_2O interface. (*A*) A set of SF spectra in the OD stretching region for the methane–water interface under 8.0 MPa of methane with temperature decreasing from 20.6 °C down to −0.5 °C. Times at which spectra at different temperatures were taken after start of cooling are indicated. (*Inset*) Representative theoretical fit (gray) of the SF spectrum (black) at 1.6 °C and the imaginary components (dotted curves) of the 3 modes composing the spectra. The amplitudes of the 3 modes as functions of temperature deduced from fitting of the SF intensity spectra are presented in *B* for 8.0 MPa and *C* for 6.0 MPa of methane vapor pressure. The black dashed vertical lines mark the temperature ranges of 3 different stages of structural changes at the methane–water interface. The colored dashed lines serve as a guide to the eye. The phase equilibrium temperatures under 8.0 and 6.0 MPa are ~14.0 and ~11.5 °C, respectively (46).

suggested by MD simulations (23). In stage I (above 14.7 ± 0.5 °C), more methane molecules are dissolved into the interfacial water layer at lower temperature. The higher methane concentration would increase the contact area of the methane–water interface and lead to a stronger SF spectrum (42), as seen by the increase of the 2,370 cm^{-1} and the 2,535 cm^{-1} modes. In stage II (between 10 and 14.7 °C), the composition and structure of the interface hardly change, as judged from the hardly perceptible spectral variation. This marks the incubation stage where methane–water complexes as nuclei (or the labile "blobs" proposed by MD simulations) for

growth of methane clathrate appear in dynamical equilibrium with surrounding. Like nuclei in crystal growth, they constitute only a tiny fraction of the interfacial layer, but the fraction increases as temperature is lowered. Their presence is difficult to detect from the change of the bonded-OD stretch spectrum, but can be seen from the emergence of a mode in the dangling-OD stretch region as we shall describe later. In stages III (below ~10 °C), the appearance of the 2350 cm^{-1} mode in Fig. 2*B* that causes the redshift of the LFB in Fig. 2*A* suggests that some of the nuclei must have reached the critical size and are now able to grow into methane clathrate. The growth is stronger at lower temperature as evidenced by the increasing amplitude of the clathrate mode at 2,350 cm^{-1} with decreasing temperature in Fig. 2*B*. This growth of clathrate is at the expense of nonparticipating interfacial water molecules, and accordingly, the amplitudes of the 2,370 cm^{-1} mode and the 2,535 cm^{-1} mode drop in correlation with the growth of the clathrate mode.

A similar methane clathrate evolution process, described in Fig. 2*C*, was observed with the methane pressure kept at 6.0 MPa (the measured SF spectra are presented in *SI Appendix*, Fig. S2). As expected, stage II starts at a lower temperature around 12.5 °C, signifying that under lower pressure, the methane–water complexes emerge at lower temperature. However, the starting temperature of stage III appears to be very close to the corresponding one at 8.0 MPa. This is likely to be associated with an intrinsic property of water. We noticed that the temperature of maximum density (TMD, T_{MD}) for D_2O is at 11.6 °C, and suspected that the expansion and increasing order of the H-bonding network of water below T_{MD} may promote the growth of methane–water complex into methane clathrate. The idea was supported by the observation that for the methane–H_2O interface, stage III started also around T_{MD} (= 3.98 °C) of H_2O (*SI Appendix*, Fig. S3).

Observation of a Dangling-OD Mode for Methane–Water Complexes. We also took the SF spectra in the dangling-OD stretching region of the methane–water interface at different temperatures in a time sequence under 8.0 MPa methane vapor pressure. They are displayed in Fig. 3*A*. At temperature above 15.5 and 23 °C (in stage I), the spectrum shows the usual dangling-OD peak at 2,720 cm^{-1}, but at 12.0 and 5.7 °C (in stages II and III, respectively), the strength of the dangling-OD mode is lower, and a mode at ~2,660 cm^{-1} emerges. According to MD simulations, the smaller 5^{12} water cages would appear during the early stages of nucleation, followed by emergence of the $5^{12}6^2$ cages (6). We conducted a density-functional theory (DFT) calculation on an individual 5^{12} cage with a methane molecule embedded (sketched in the inset of Fig. 3*B*) to find its IR and Raman vibrational spectra in the OD stretching region (*SI Appendix*, Fig. S5), of which the part near the dangling-OD mode is depicted in Fig. 3*B*. It is seen that an antisymmetry O-D stretching mode appears at ~2,660 cm^{-1}, close to the frequency of our experimentally observed mode. (See detailed description of the calculation in *SI Appendix*.) While the agreement may be fortuitous, the appearance of this mode seems to signify the emergence of the cage-like methane–water structure at the interface as nucleus of clathrate growth. We did a similar calculation on the $5^{12}6^2$ cage, but unfortunately, its stretching vibrational modes overlap with the broad OH stretching band of liquid water and are difficult to resolve. As signature of the nucleus, the 2,660 cm^{-1} mode was expected to have an incubation time to emerge. We monitored, at given temperature, the growth of the mode in time. Indeed, as presented in Fig. 3*C*, the result shows that the incubation time for the mode is much longer at higher temperature. At 4.7 °C in stage III, the mode appears almost right away and saturated in amplitude (with respect to the measurement time). At 10 °C near the boundary between stages II and III, it takes about 4 h to emerge and reach a lower saturation. At 14.5 °C near the boundary between stages I and II, it takes 12 h to show up and 13 h to reach a low saturation. This observation provides a timescale on how long it takes for the formation (and disintegration) of the cage-like methane–water complex to reach dynamical equilibrium. To correlate further the mode with clathrate formation, we first grew the solid methane clathrate at 5.7 °C by gently stirring the methane–water system, and then melting it and bringing it to 14.5 °C. The mode at ~2,660 cm^{-1} persisted in the heating process, and appeared almost as strong as that at 5.7 °C before the solid clathrate was grown, as shown in Fig. 3*D*. This observation indicates that upon dissociation of methane clathrate, nuclei with cage-like structure remain stable in the melt; they are ready to help recrystallization of clathrate, and could explain the so-called memory effect described earlier.

Structural Hysteresis at the Methane–Water Interface during Cooling–Heating Cycle. As the reversed process of cooling, heating would first disintegrate the crystalline methane clathrate into methane–water complexes and water and then reduce the methane concentration in the interfacial water layer (stage III to I). This was also observed by SFVS. Amplitude variations of the 2 low-frequency modes at 2,350 cm^{-1} and 2,370 cm^{-1} (representing clathrate structure and water structure, respectively) are plotted in Fig. 4 *A* and *B* with increasing temperature for the methane–water

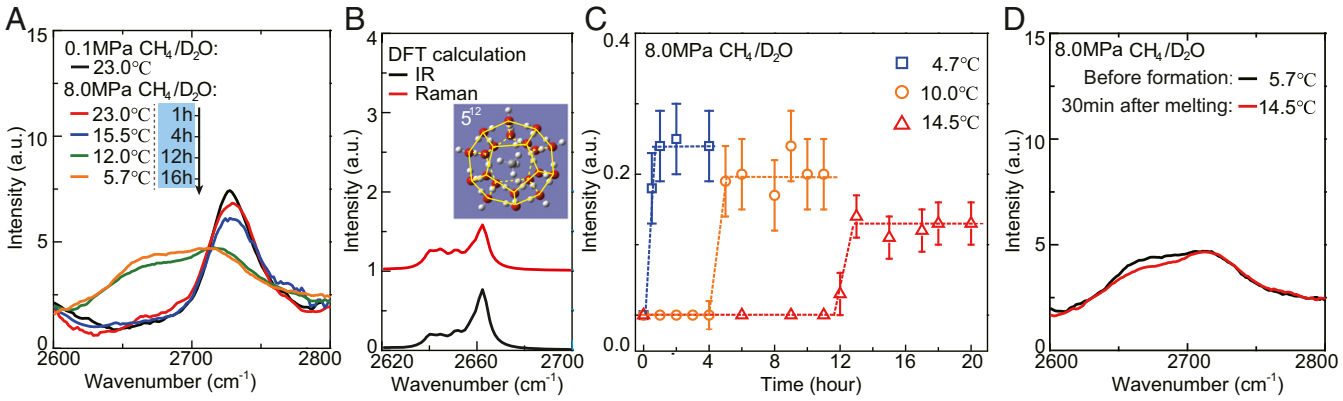

Fig. 3. OH stretching mode of 5^{12} (12 pentagons) water cages with embedded methane. (*A*) SF spectra in the dangling-OD stretching region for the methane–water interface at different temperatures. A vibrational mode centered at ~2,660 cm^{-1} can be identified in the spectra for 12.0 and 5.7 °C. Times when the spectra were taken after start of cooling are indicated. (*B*) Calculated IR and Raman spectra in the 2,620 to 2,700 cm^{-1} range for a 5^{12} methane-embedded water cage with molecular structure shown (*Inset*). (*C*) Evolution of the 2,660 cm^{-1} mode in time under different temperatures. (*D*) SF spectra of the methane–water interface on cooling to 5.7 °C (black curve) and on heating to 14.5 °C after melting of solid methane clathrate (red curve).

interface under 8.0 MPa, together with those from the cooling process. The plots exhibit a hysteresis behavior. As temperature increases from 0 °C, the amplitudes of the 2 modes remain unchanged within experimental uncertainty, signifying little dissembling of methane clathrate, until ~10 °C. The 2,350 cm^{-1} clathrate mode then decreases and the 2,370 cm^{-1} mode increases with increase of temperature, indicating disintegration of clathrates. The clathrate mode completely disappears at ~14 °C when all clathrates are disintegrated, and the SF spectrum now resembles that of the system in stage II reached upon cooling, and it persists until 22 °C. Above 22 °C, the spectrum shows that the system is in stage I with methane molecular concentration in the interfacial water layer decreasing with increasing temperature. The hysteresis behavior of cooling and heating is similar to that of bulk methane clathrate (2, 14). We note that irrespective of whether the system is first cooled down to 0 °C (in stage III) or 12 °C (in stage II), the spectral variation with increasing temperature from stage II into stage I is nearly the same. This is seen by comparing Fig. 4 *B* and *C*. Apparently, once the cage-like nuclei are formed in water by cooling, they can exist in heating to an appreciably higher temperature. This again is a manifestation of the so-called memory effect (14, 22, 29, 30, 43), that is, solid clathrate is more readily formed in methane–water solution prepared by melting of solid clathrate. The nuclei that do not exist in freshly prepared solution at a given temperature may be present in melted solution at the same temperature.

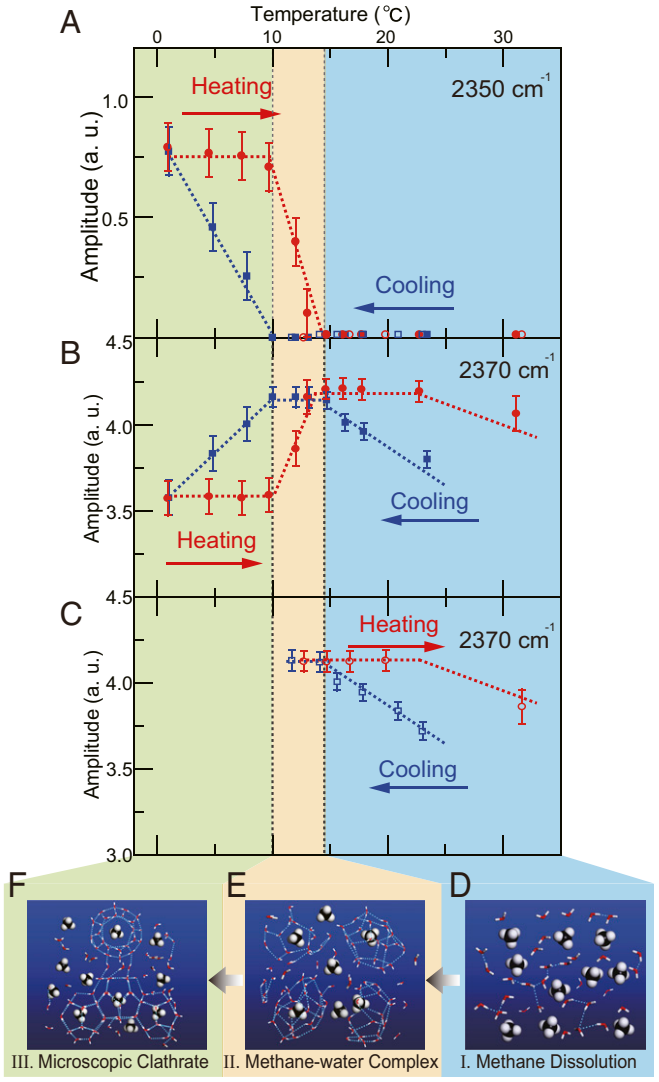

Fig. 4. Formation/disintegration of methane clathrate showing structural hysteresis during cooling–heating cycles. Amplitude of (*A*) the 2,350 cm^{-1} mode and (*B*) the 2,370 cm^{-1} mode versus temperature of the methane–water interface that was first cooled (blue color) down to 0 °C and then heated up to 31 °C (red color), all under fixed methane vapor pressure of 8.0 MPa. (*C*) Same as *B*, but with temperature first cooled down to 12 °C. Formation of methane clathrate appears to go through the successive stages of molecular arrangement, I to III, sketched in *D*–*F*. The phase equilibrium temperature under 8.0 MPa is ~14.0 °C (46).

Summary

We have used surface-specific SFVS to study nucleation and dissociation of methane clathrate. We confirmed that with water under high-pressure methane vapor, nucleation and growth of methane clathrate starts at the methane–water interface. We found, from spectral variation of the interface in the OH/OD stretching range with temperature, that similar to crystal growth, the methane–water interfacial structure undergoes 3 stages of changes. We must first have sufficient amount of methane molecules dissolved in water. This can happen under high methane vapor pressure in the MPa range; the higher the pressure, the more is the solvated methane concentration. Then, with sufficient methane concentration in water, methane clathrate can grow under sufficiently low temperature. In the first stage with a fixed high-vapor pressure, the solvated methane concentration increases with decrease of temperature. In the second stage, a cage-like structure of water with an embedded methane molecule seems to appear in dynamical equilibrium with water and serve as nuclei or seeds for later possible growth of methane clathrate, while the host water structure remains nearly unchanged. In the third stage, some of the nuclei in the interfacial layer reach the critical size and grow into methane clathrate. Fig. 4 *D*–*F* are sketches describing the molecular arrangement of the 3 stages, respectively. Previous MD simulations (23, 24) suggested that methane clathrate would first appear in an amorphous phase, and then transform into a crystalline phase. With nuclei already reaching critical size in stage III, slight external perturbation of the methane–water mixture can drastically speed up the growth of macroscopic methane clathrate. We observed that with the methane–water interfacial system in stage III, weak stirring of the water led to rapid growth of solid methane clathrate into the bulk.

The nucleation and growth process of other clathrates of small water-insoluble molecules should be similar to what we have described here for methane clathrate although dependence on vapor pressure and temperature may vary. In all cases, nucleation tends to start at gas–water interfaces. First, a critical density of gas molecules must be dissolved into the interfacial water layer under pressure. Second, molecule–water complex must be formed to serve as embryo for further growth into clathrates. Third, conditions must exist for these embryos to grow and reach a critical size for the system to grow into macroscopic clathrates. We have demonstrated in this work that SFVS is a viable tool to monitor such a nucleation process of clathrates at the gas–water interface. The information obtained from our measurements can shed light on the various mechanisms that may promote or inhibit formation of clathrates, which are relevant to some most important energy and environmental issues.

The existence of cage-like methane–water complexes as embryos in stage II is obviously most interesting. More work is yet to be carried out to learn how growth and final stabilization of such complexes, as featured by the additional vibrational mode next to the dangling OH/OD mode of water, depend on temperature and time, especially near the boundaries of stages I and II and stages II and III. How it correlates with the characteristic OH/OD stretching mode for methane clathrate is also to be investigated. A careful study of the latter on how long it takes to reach equilibrium at different temperatures should also be in order.

Methods and Materials

Broadband SFVS. The broadband SFVS scheme with a femtosecond laser system (44) was adopted in our measurements with s-, s-, and p- polarizations for the sum-frequency output, the visible input, and the IR input beams, respectively. The incident angles of visible and IR beams are 45° and 40°, respectively. The broadband IR input spanning over the wavelength range of 2,200 to 2,800 cm^{-1} with ∼0.5-μJ/pulse [weak enough to avoid heating at the interface (45)] and the narrowband visible input at 800 nm with 8 μJ/pulse were focused through the top window of the chamber onto the sample with spot diameters of 200 and 220 μm, respectively. The SF signal was collected in reflection geometry and detected with an electron multiplying charge coupled device (EMCCD) camera (DU970P-UVB Newton, Andor) after a set of interference filters and a spectrograph.

The methane–D_2O sample was placed in a chamber that could have the methane gas pressure tuned from 0.1 to 10.0 MPa and temperature varied between −10 and 60 °C. Before measurement of each SF spectrum, the sample was kept under the selected pressure and temperature for ∼1 h.

High-Pressure Chamber. A stainless chamber with optical windows was constructed to be used at pressure up to 10.0 MPa. High-pressure gas was injected into the chamber from a gas cylinder after going through a 30 nm particle filter. Temperature of the chamber was controlled by circulating coolant in a copper pipe attached to the chamber sidewalls, and could be varied from −10 to 60 °C. Two sapphire or fused silica windows were mounted on the top and bottom of the chamber, allowing reflected SFVS and backward Raman scattering spectroscopy measurements.

Preparation of Polycrystalline Methane Clathrate. Deuterated water (D_2O, purity 99.9%, Cambridge Isotope Laboratories, Inc.) and methane (CH_4, purity 99.999%) were used for growth of methane clathrate in the high-pressure chamber. With the chamber kept at 5 °C, the methane pressure at 4.0 MPa, and water mildly perturbed by a Teflon-coated magnetic stirrer, growth of polycrystalline methane clathrate was observed. If the chamber was slightly tilted and water partially touching the top window, a thin film of the clathrate was found to have covered part of the top window and was used for the reflected SFVS and Raman measurements.

Sample Preparation for Experiment at Gas–Water Interface. Ultrapure deionized H_2O (18.2 MΩ·cm) or deuterated water (D_2O, purity 99.9%, Cambridge Isotope Laboratories, Inc.) was held in a fused silica cell placed inside the high-pressure chamber (*SI Appendix*, Fig. S1). The water cell, sapphire- or fused silica windows, and all glass wares used in the experiment were cleaned by soaking in a mixture of concentrated sulfuric acid (98%) and NoChromix (Godax Laboratories Inc., ∼4 g/100 mL) for a few hours, then rinsed thoroughly with ultrapure deionized water (18.2 MΩ·cm, Thermo-Fisher) and finally dried by baking at 120 °C. Ultrapure methane (purity 99.999%) and nitrogen (purity 99.9999%) gases were used after going through a 30 nm particle filter in this study.

Data Availability Statement. All data are included in the manuscript and *SI Appendix*.

ACKNOWLEDGMENTS. C.T. acknowledges support from the National Key Research and Development Program of China (2016YFA0300902 and 2016YFC0202802) and the National Natural Science Foundation of China Grants 11290161 and 11874123. Y.S. acknowledges support from the National Natural Science Foundation of China, Grant 21803012 and the China Postdoctoral Science Foundation Grant 2018M630394.

1. E. D. Sloan, F. Fleyfel, A molecular mechanism for gas hydrate nucleation from ice. *AIChE J.* **37**, 1281–1292 (1991).
2. R. L. Christiansen, E. D. Sloan, Mechanisms and kinetics of hydrate formation. *Ann. N. Y. Acad. Sci.* **715**, 283–305 (1994).
3. C. Moon, P. C. Taylor, P. M. Rodger, Molecular dynamics study of gas hydrate formation. *J. Am. Chem. Soc.* **125**, 4706–4707 (2003).
4. E. D. Sloan, Jr, Fundamental principles and applications of natural gas hydrates. *Nature* **426**, 353–363 (2003).
5. Y. Park *et al*., Sequestering carbon dioxide into complex structures of naturally occurring gas hydrates. *Proc. Natl. Acad. Sci. U.S.A.* **103**, 12690–12694 (2006).
6. M. R. Walsh, C. A. Koh, E. D. Sloan, A. K. Sum, D. T. Wu, Microsecond simulations of spontaneous methane hydrate nucleation and growth. *Science* **326**, 1095–1098 (2009).
7. C. A. Koh, E. D. Sloan, A. K. Sum, D. T. Wu, Fundamentals and applications of gas hydrates. *Annu. Rev. Chem. Biomol. Eng.* **2**, 237–257 (2011).
8. Z. M. Aman, C. A. Koh, Interfacial phenomena in gas hydrate systems. *Chem. Soc. Rev.* **45**, 1678–1690 (2016).
9. P. Warrier, M. N. Khan, V. Srivastava, C. M. Maupin, C. A. Koh, Overview: Nucleation of clathrate hydrates. *J. Chem. Phys.* **145**, 211705 (2016).
10. M. Maslin *et al*., Gas hydrates: Past and future geohazard? *Philos. Trans. R. Soc. A-Math. Phys. Eng. Sci.* **368**, 2369–2393 (2010).
11. P. G. Brewer, G. Friederich, E. T. Peltzer, F. M. Orr, Jr, Direct experiments on the ocean disposal of fossil fuel CO2. *Science* **284**, 943–945 (1999).
12. K. A. Kvenvolden, Potential effects of gas hydrate on human welfare. *Proc. Natl. Acad. Sci. U.S.A.* **96**, 3420–3426 (1999).
13. M. Khurana, Z. Y. Yin, P. Linga, A review of clathrate hydrate nucleation. *ACS Sustain. Chem.& Eng.* **5**, 11176–11203 (2017).
14. E. D. Sloan, C. A. Koh, *Clathrate Hydrates of Natural Gases* (CRC Press, ed. 3, 2008).
15. T. Yagasaki, M. Matsumoto, H. Tanaka, Adsorption mechanism of inhibitor and guest molecules on the surface of gas hydrates. *J. Am. Chem. Soc.* **137**, 12079–12085 (2015).
16. R. Radhakrishnan, B. L. Trout, A new approach for studying nucleation phenomena using molecular simulations: Application to CO2 hydrate clathrates. *J. Chem. Phys.* **117**, 1786–1796 (2002).
17. B. C. Knott, V. Molinero, M. F. Doherty, B. Peters, Homogeneous nucleation of methane hydrates: Unrealistic under realistic conditions. *J. Am. Chem. Soc.* **134**, 19544–19547 (2012).
18. P. Pirzadeh, P. G. Kusalik, Molecular insights into clathrate hydrate nucleation at an ice-solution interface. *J. Am. Chem. Soc.* **135**, 7278–7287 (2013).
19. N. J. English, J. M. D. MacElroy, Perspectives on molecular simulation of clathrate hydrates: Progress, prospects and challenges. *Chem. Eng. Sci.* **121**, 133–156 (2015).
20. E. D. Sloan, Conference overviewa. *Ann. N. Y. Acad. Sci.* **715**, 1–23 (1994).
21. M. Sugaya, Y. H. Mori, Behavior of clathrate hydrate formation at the boundary of liquid water and a fluorocarbon in liquid or vapor state. *Chem. Eng. Sci.* **51**, 3505–3517 (1996).
22. J. A. Ripmeester, S. Alavi, Some current challenges in clathrate hydrate science: Nucleation, decomposition and the memory effect. *Curr. Opin. Solid State Mater. Sci.* **20**, 344–351 (2016).
23. L. C. Jacobson, W. Hujo, V. Molinero, Amorphous precursors in the nucleation of clathrate hydrates. *J. Am. Chem. Soc.* **132**, 11806–11811 (2010).
24. L. C. Jacobson, W. Hujo, V. Molinero, Nucleation pathways of clathrate hydrates: Effect of guest size and solubility. *J. Phys. Chem. B* **114**, 13796–13807 (2010).
25. M. Lauricella, S. Meloni, N. J. English, B. Peters, G. Ciccotti, Methane clathrate hydrate nucleation mechanism by advanced molecular simulations. *J. Phys. Chem. C* **118**, 22847–22857 (2014).
26. T. Koga *et al*., Hydrate formation at the methane/water interface on the molecular scale. *Langmuir* **26**, 4627–4630 (2010).
27. L. Boewer *et al*., On the spontaneous formation of clathrate hydrates at water–guest interfaces. *J. Phys. Chem. C* **116**, 8548–8553 (2012).
28. C. A. Koh, R. P. Wisbey, X. Wu, R. E. Westacott, A. K. Soper, Water ordering around methane during hydrate formation. *J. Chem. Phys.* **113**, 6390–6397 (2000).
29. P. Buchanan *et al*., Search for memory effects in methane hydrate: Structure of water before hydrate formation and after hydrate decomposition. *J. Chem. Phys.* **123**, 164507 (2005).
30. H. Thompson *et al*., Methane hydrate formation and decomposition: Structural studies via neutron diffraction and empirical potential structure refinement. *J. Chem. Phys.* **124**, 164508 (2006).
31. T. Uchida, R. Okabe, S. Mae, T. Ebinuma, H. Narita, "In situ observations of methane hydrate formation mechanisms by Raman spectroscopy" *Gas Hydrates: Challenges for the Future, Annals of the New York Academy of Sciences*, G. D. Holder, P. R. Bishnoi, Eds. (New York Academic Sciences, New York, 2000), vol. 912, pp. 593–601.
32. A. K. Sum, R. C. Burruss, E. D. Sloan, Measurement of clathrate hydrates via Raman spectroscopy. *J. Phys. Chem. B* **101**, 7371–7377 (1997).
33. J. A. Ripmeester, C. I. Ratcliffe, On the contributions of NMR spectroscopy to clathrate science. *J. Struct. Chem.* **40**, 654–662 (1999).
34. S. Gao, W. House, W. G. Chapman, NMR/MRI study of clathrate hydrate mechanisms. *J. Phys. Chem. B* **109**, 19090–19093 (2005).
35. Y. R. Shen, *Fundamentals of Sum-Frequency Spectroscopy* (Cambridge University Press, 2016).
36. S. Subramanian, E. D. Sloan, Molecular measurements of methane hydrate formation. *Fluid Phase Equilib.* **158**, 813–820 (1999).
37. M. Sovago *et al*., Vibrational response of hydrogen-bonded interfacial water is dominated by intramolecular coupling. *Phys. Rev. Lett.* **100**, 173901 (2008).
38. C. S. Tian, Y. R. Shen, Isotopic dilution study of the water/vapor interface by phase-sensitive sum-frequency vibrational spectroscopy. *J. Am. Chem. Soc.* **131**, 2790–2791 (2009).
39. X. Wei, P. B. Miranda, Y. R. Shen, Surface vibrational spectroscopic study of surface melting of ice. *Phys. Rev. Lett.* **86**, 1554–1557 (2001).
40. A. van Cleeff, G. A. M. Diepen, Gas hydrates of nitrogen and oxygen. *Rec.Trav.Chim.* **79**, 582–586 (1960).
41. G. J. Guo, P. M. Rodger, Solubility of aqueous methane under metastable conditions: Implications for gas hydrate nucleation. *J. Phys. Chem. B* **117**, 6498–6504 (2013).
42. S. Strazdaite, J. Versluis, E. H. Backus, H. J. Bakker, Enhanced ordering of water at hydrophobic surfaces. *J. Chem. Phys.* **140**, 054711 (2014).
43. P. M. Rodger, Methane hydrate–Melting and memory. *Ann. N. Y. Acad. Sci.* **912**, 474–482 (2000).
44. Y. C. Wen *et al*., Unveiling microscopic structures of charged water interfaces by surface-specific vibrational spectroscopy. *Phys. Rev. Lett.* **116**, 016101 (2016).
45. Y. Xu *et al*., Theoretical analysis and simulation of pulsed laser heating at interface. *J. Appl. Phys.* **123**, 025301 (2018).
46. X. P. Wang, A. J. Schultz, Y. Halpern, Kinetics of methane hydrate formation from polycrystalline deuterated ice. *J. Phys. Chem. A* **106**, 7304–7309 (2002).